

MULTI-FREQUENCY VARIABILITY STUDY OF TON 599 DURING HIGH ACTIVITY OF 2017

RAJ PRINCE¹

¹Raman Research Institute, Sadashivanagar, Bangalore 560080, India

Draft version December 13, 2018

ABSTRACT

In this work, I have presented a multi-frequency variability and correlation study of the blazar Ton 599, which was observed first time in flaring state at the end of 2017. Data from *Fermi*-LAT, Swift-XRT/UVOT, Steward Observatory, and OVRO (15 GHz) is used, and it is found that the source is more variable in γ -ray and optical/UV than X-ray and radio. Large variations in the degree of polarization (DoP) and position angle (PA) is noticed during the flaring period. Maximum flux during γ -ray flare is found to be 12.63×10^{-7} at MJD 58057.5 from the 1-day bin light curve (LC), which is the maximum flux ever achieved by this source. It is further found that all the peaks of flare are very symmetric, which suggests the cooling time of electrons is much smaller than light crossing time. Using 1-day as a fast variability time, the size of the γ -ray emission region is estimated as 1.88×10^{16} cm. Two 42 GeV of photons are detected during the flare which puts a constraint on the location of the emission region, and it is found that the γ -ray emitting blob is located at the outer edge or outside the broad line region (BLR). A trend of increasing fractional variability towards higher energies is also seen. Strong correlations were seen between γ -ray, optical/UV, X-ray, and radio (15 GHz) emission. A small time lag between γ -ray and optical/UV suggest their emission to be co-spatial while lag of 27 days between γ -ray and OVRO (15 GHz) suggest two different emission zone separated by a distance of ~ 5 pc.

Keywords: galaxies: active; gamma rays: galaxies; individuals: Ton 599

1. INTRODUCTION

Blazars are thought to be radio-loud active galactic nuclei (AGNs) which have jets oriented close to the observer line of sight (Urry & Padovani 1995). They emit in all frequencies extending from radio to very high energy γ -rays. In general, Blazars shows minutes (Aharonian et al. 2007) to years (Raiteri et al. 2013) scale of variability time across the entire electromagnetic spectrum. Their spectral energy distribution (SED) is characterized by two hump kind of structures. The first one peaks in low energy band (IR to soft X-ray), which is well explained by synchrotron emission caused by relativistic electrons in the magnetic field of the jets and the second one peaks in the high energy band (hard X-ray to γ -ray), which is thought to be the product of inverse Compton scattering of low energy photon within the jets called Synchrotron self Compton (Konigl 1981; Marscher & Gear 1985; Ghisellini & Tavecchio 2009) or from outside the jets (External Compton; EC) with relativistic electrons. There is also an alternative way that can produce the high energy hump through the hadronic process in which high energy protons interact with low energy protons and produce charge and neutral muons, and that can decay into high energy γ -ray and neutrinos. In leptonic scenarios, the external seed photons can come from direct disk emission, BLR, dusty or molecular torus (Bottcher 2007).

Ton 599 is a FSRQ also known as 4C 29.45, and 3FGL J1159.5+2914 (Acero et al. 2015) with RA = 179.8826413 deg, Dec = 29.2455075 deg, and $z = 0.72449$.

This is the first time the source has gone through a long flaring state across the entire electromagnetic spectrum. Many correlation studies have been done, between optical, X-ray and γ -ray to discussed the connection between their emission regions, in FSRQ. Cohen et al. (2014) have studied the correlation between optical and γ -ray for 40 Blazars and they found that high energy emission leads the low energy emission with a time lag of 1-10 days. A correlation study of a sample of 183 blazars have also been done by Pushkarev et al. (2010) and they found that in most of the cases radio flare lags the gamma-ray flare. It is also true that the time delay between flares of two bands depends on their separation (Fuhrmann et al. 2014). In blazar, the exact location of the gamma-ray emission region is not known because of the poor angular resolution in high energy. While on the other hand, the radio emission region has been resolved in the jets of blazar with milliarcsecond resolution of radio observations. Ramakrishnan et al. (2014) have also been studied the correlation between γ -ray and radio emission for this source and they found that γ -ray is lagging behind the radio with a time lag of 120 days, and that constrains the gamma-ray emission region in the parsec-scale jet.

In this paper, I have studied the correlation between optical, X-ray and gamma-ray to understand the multi-waveband emission during the flare of 2017.

2. MULTIWAVELENGTH OBSERVATIONS AND DATA ANALYSIS

2.1. *Fermi*-LAT

Fermi-LAT is a pair conversion γ -ray Telescope sensitive to photon energies between 20 MeV to higher than 500 GeV, with a field of view of about 2.4 sr

(Atwood et al. 2009). The LAT’s field of view covers about 20% of the sky at any time and it scans the whole sky every three hours. The instrument was launched by NASA in 2008 into a near earth orbit. Ton 599 was continuously monitored by *Fermi*-LAT since 2008 August. The standard data reduction and analysis procedure¹ has been followed. Other analysis procedure is the same as given in Prince et al. (2018). I have analyzed the *Fermi*-LAT data from Jan 2014 to Jan 2018 and found that most of the time source was in quiescent state and started showing major activity at the end of 2017 (Figure 1). At the end of 2015, it shows the flux rising, but that does not last for a long time and also the maximum flux was $\sim 4 \times 10^{-7}$ ph cm⁻² s⁻¹.

2.2. *Swift*-XRT/UVOT

Ton 599 was observed by *Swift*-XRT/UVOT during flaring state. Details of the observations are present in Table 1. Cleaned event files were obtained using the task ‘*artpipeline*’ version 0.13.2. Latest calibration files (CALDB version 20160609) and standard screening criteria were used for re-processing the raw data. Cleaned event files corresponding to the Photon Counting (PC) mode were considered. Circular regions of radius 20 arc seconds centered at the source and slightly away from the source were chosen for the source and the background regions respectively while analyzing the XRT data. The X-ray spectra were extracted in *xselect*. The obtained spectra is fitted using simple power law model with the galactic absorption column density $n_H = 1.77 \times 10^{20}$ cm⁻² (Kalberla et al. 2005). The *Swift* Ultraviolet/Optical Telescope (UVOT, Roming et al. 2005) also observed Ton 599 in all the six filters U, V, B, W1, M2, and W2. The source image was extracted from a region of 5 arc seconds centered at the source. The background region was chosen with a radius of 10 arcseconds away from the source from a nearby source free region. The ‘*uvotsource*’ task has been used to extract the source magnitudes and fluxes. Magnitudes are corrected for galactic extinction (Schlafly et al. 2011) and converted into flux using the zero points (Breeveld et al. 2011) and conversion factors (Larionov et al. 2016).

2.3. *Steward Optical Observatory*

I have also used the archival data from the *Steward* optical observatory, Arizona (Smith et al. 2009)². Ton 599 is being continuously monitored with the SPOL CCD Imaging/Spectrometer as a part of *Fermi* multi-wavelength support programme. Optical V-band and R-band photometric data is used along with the Polarimetric (degree of polarization and position angle) data for the whole flaring period during the end of 2017.

2.4. *OVRO data at 15 GHz*

Ton 599 is also observed in radio by Owens Valley Radio Observatory (OVRO; Richards et al. (2011) as a part of *Fermi* monitoring programme. I have collected the radio data at 15 GHz during MJD 58040 – 58120.

3. RESULTS AND DISCUSSIONS

¹ <https://fermi.gsfc.nasa.gov/ssc/data/analysis/documentation/>

² <http://james.as.arizona.edu/~psmith/Fermi/>

Table 1

Table shows the log of the observations during the flaring state (MJD 58040 – 58120).

Observatory	Obs-ID	Exposure (ks)
Swift-XRT/UVOT	00036381023	2.48
Swift-XRT/UVOT	00036381024	2.53
Swift-XRT/UVOT	00036381025	2.46
Swift-XRT/UVOT	00036381026	2.47
Swift-XRT/UVOT	00036381027	2.40
Swift-XRT/UVOT	00036381028	1.61
Swift-XRT/UVOT	00036381030	2.20
Swift-XRT/UVOT	00036381031	2.27
Swift-XRT/UVOT	00036381032	1.58
Swift-XRT/UVOT	00036381033	1.65
Swift-XRT/UVOT	00036381034	1.67
Swift-XRT/UVOT	00036381035	1.99
Swift-XRT/UVOT	00036381036	0.99
Swift-XRT/UVOT	00036381037	1.94
Swift-XRT/UVOT	00036381038	2.02
Swift-XRT/UVOT	00036381040	1.92
Swift-XRT/UVOT	00036381041	0.90
Swift-XRT/UVOT	00036381042	0.87
Swift-XRT/UVOT	00036381044	1.73
Swift-XRT/UVOT	00036381046	1.84
Swift-XRT/UVOT	00036381047	1.94
Swift-XRT/UVOT	00036381048	1.93

I have analyzed the *Fermi*-LAT data from Jan 2014 to Jan 2018 (MJD 56751 – MJD 58140). The light curve of the source along with the photon index during these four years is shown in Figure 1. It is clear that most of the time source is in quiescence state where flux is very low (close to zero) and sometimes it shows high flux state. Rise in the flux with spectral hardening is observed during the end of 2015 with flux reaching the value $\sim 4 \times 10^{-7}$ ph cm⁻² s⁻¹. After 2015 Ton 599 was in more or less a quiescence state with some small fluctuations in 2016. In 2017 it started showing activity and at the end of 2017 the source under-went clear major flares. Zoomed version of the flare is shown in the right panel of Figure 1 and a period has been chosen just before the flare when the source is in quiescence and called it pre-flare. I have studied this major flare along with the multi-wavelength observations and done the fractional variability and correlation studies among different wavelength during the flaring period (MJD 58040 – MJD 58120).

Gamma-ray spectral analysis is also done, four spectral models mentioned in Prince et al. (2018) are used to fit the gamma-ray spectral energy distributions (SEDs).

3.1. *Multi-wavelength light curves*

Multi-wavelength light curve of Ton 599 during the flaring episode MJD 58040 – MJD 58120 is shown in Figure 2. The first panel shows the 1-day binning of *Fermi*-LAT data. As we have seen in Figure 1 the source started showing the activity at the end of 2017. In Figure 2, the flux started rising after MJD 58040 and lasted for around two and a half months and again got back to its quiescence state after MJD 58120. The flux started rising very slowly and it took around twenty days to become a full-fledged flare. The source showed a clear and major peak at MJD 58057.5 and the maximum flux attained is $\sim 13 \times 10^{-7}$ ph cm⁻² s⁻¹ from one day binning. After the major peak, the source was in a higher state for almost two months with an average flux of 6.69×10^{-7}

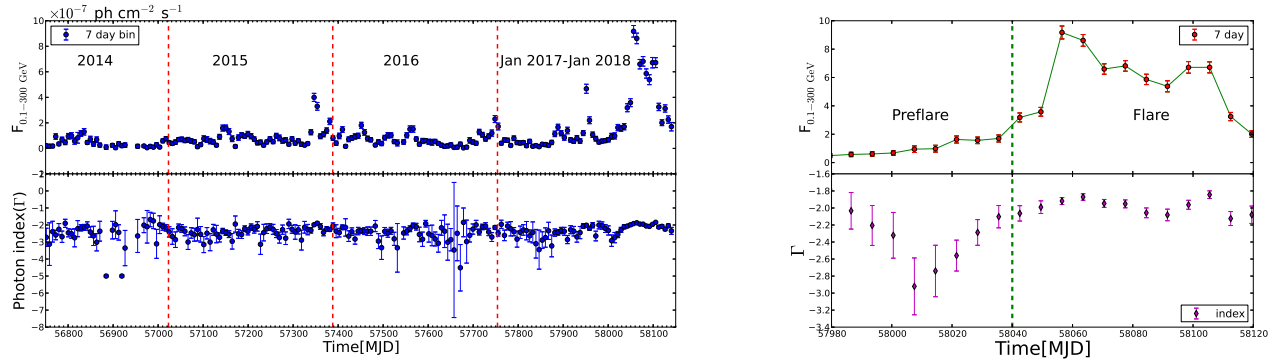


Figure 1. left: Light curve of Ton 599 from Jan 2014 to Jan 2018. right: Zoomed version of flare at the end of 2017 and vertical green dashed line separating the two state of the source.

$\text{ph cm}^{-2} \text{s}^{-1}$.

Swift-XRT/UVOT observations were carried out when the source was already in flaring state. All the details about the observations are mentioned in Table 1. XRT light curve for 2.0–10.0 keV are shown in the second panel of Figure 2. The source shows the higher state in X-ray, and its first peak coincides with the γ -ray peak at MJD 58058 with a flux of $3.80 \times 10^{-12} \text{ erg cm}^{-2} \text{ s}^{-1}$. X-ray flux shows fluctuating behavior during the γ -ray flare and it settled down in its quiescence state as the γ -ray flare ended. The quiescence state flux is noted as $0.87 \times 10^{-12} \text{ erg cm}^{-2} \text{ s}^{-1}$.

Ton 599 was also observed with UVOT in all the six filters (U, B, V, W1, M2, W2). The light curves for optical (U, B, V) and UV (W1, M2, W2) filters are shown in the third and fourth panel of Figure 2 respectively. Since Ton 599 was already flaring when Swift started looking at it, so the optical and UV fluxes were already in the high state. It shows the peak at MJD 58058 which clearly coincides with the X-ray as well as γ -ray first peak. At the peak optical U, B, V fluxes are 5.92×10^{-11} , 6.17×10^{-11} , 5.81×10^{-11} and UV W1, M2, W2 fluxes are 6.19×10^{-11} , 7.41×10^{-11} , $6.54 \times 10^{-11} \text{ erg cm}^{-2} \text{ s}^{-1}$ respectively. In the light curve, it is clearly seen that the source was very variable in both optical and UV throughout the whole flaring period similar to the γ -ray. Optical and UV also follow the last peak of γ -ray flare at MJD 58103. After two months of flaring period optical and UV, flux attained its quiescence state with a flux close to zero at MJD 58118.

Steward V and R band magnitudes are plotted in the fifth panel of Figure 2. It is found that Ton 599 is more bright in R band than V band during the flare. The average magnitude during the flare in V and R band are 14.9 and 14.5 respectively.

In the sixth panel of Figure 2, the radio light curve is shown at 15 GHz from Owens Valley Radio Observatory (OVRO). It has been clearly seen that the source is in quiescence state in radio while it is flaring in the γ -ray and other waveband. The radio flux started rising slowly at MJD 58060 and after almost thirty days it attained the maximum flux 3.56 Jy at MJD 58089. The delay in the radio flare is investigated while studying the correlations among the different wave band in section 3.6.

The Degree of polarization (DoP) and position angle (PA) are plotted in panel seven & eight of Figure 2. Huge variation is seen in DoP and PA during the flare. In 10

days of span MJD 58070–58080, DoP varies from 4%–22% and PA varies from 30 degree–175 degree. The variation in the DoP and PA can be explained by shock-in-jet model (Marscher et al. 2008; Larionov et al. 2013; Casadio et al. 2015). In which a shock wave moving down the jet following magnetic field lines, covering only a portion of the jet’s cross section can lead to this variation in DoP and PA during the flare.

3.2. High energy photons and temporal evolution

High energy photons are also detected by *Fermi*, using the "ULTRACLEAN" class of events and 0.5° of ROI. The results are plotted in Figure 3, that shows the photons energy on y-axis and their arrival time on the x-axis. Photons of energy greater than 10 GeV and with a probability of greater than 99.5% are only shown in Figure 3. It is found that most of the photons have energy below 20 GeV and only few have been detected above 20 GeV. Two 42 GeV of photons have been detected during the flare with a probability of 99.7% and 99.8% at MJD 58065.7 and 58100 respectively.

The temporal evolution of flare has been studied here and, I have fitted the first peak of the flare, shown in Figure 4, by a sum of exponentials which provides the rise and decay time of the peak. The functional form of sum of exponentials is as follows:

$$F(t) = 2F_0 \left[\exp\left(\frac{t_0 - t}{T_r}\right) + \exp\left(\frac{t - t_0}{T_d}\right) \right]^{-1}, \quad (1)$$

where F_0 = flare amplitude at time t_0 , T_r = rise time, T_d = decay time (Abdo et al. 2010). Peak shown in Figure 4 is symmetric with rising and decay time of 2.22 ± 0.14 and 2.30 ± 0.13 days respectively. The temporal fitting is also applied for other peaks found during the flare, and most of them are found to be symmetric. The symmetric time profile is expected when the cooling time of electrons t_{cool} is much smaller than the light crossing time R/c (Chiaberge & Ghisellini 1999), where R is the size of the emission region.

In the lower panel of Figure 4, Gamma-ray fluxes are plotted with respect to the photon spectral index and a clear brighter and harder spectral behavior is seen. During this high activity, the spectral index is harder than those reported in 3FGL catalog Acero et al. (2015) for this source.

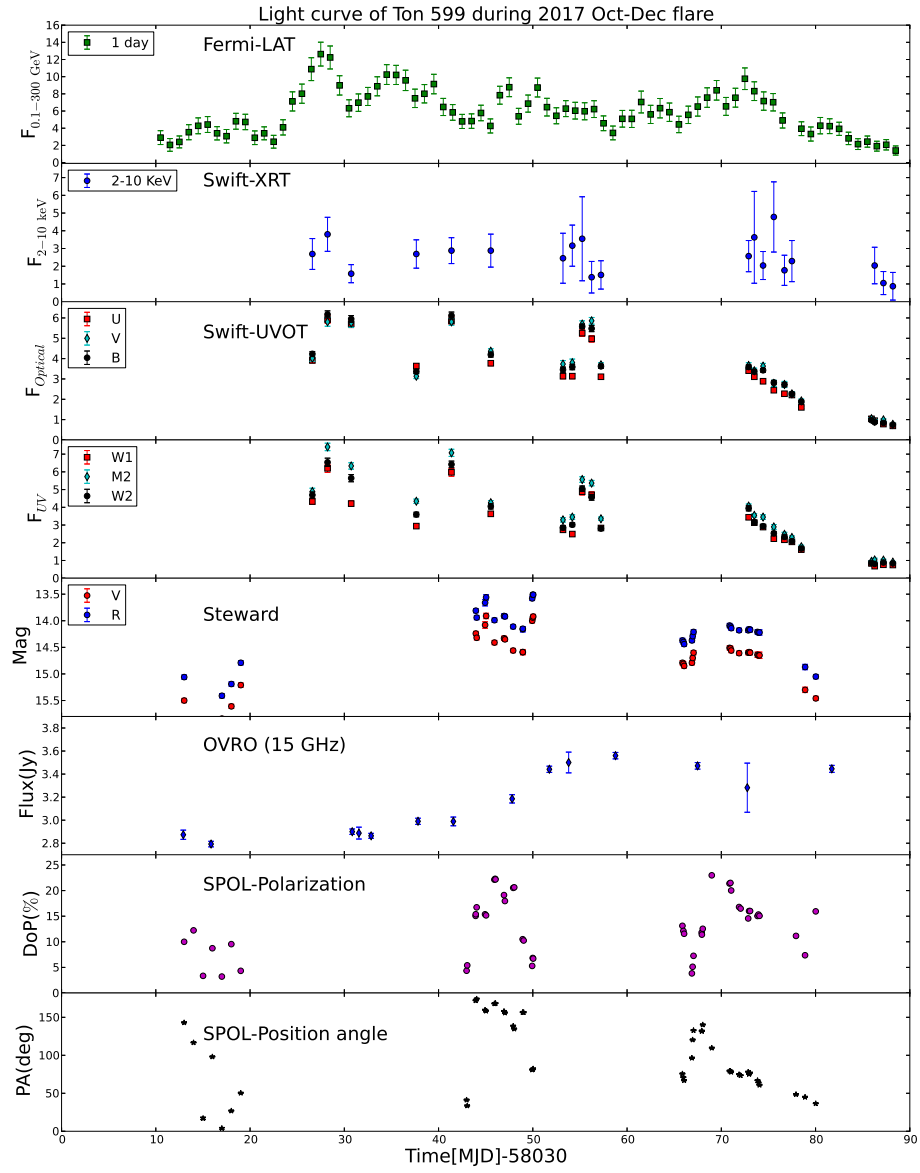


Figure 2. Multi-wavelength light curve of Ton 599 during end of 2017. *Fermi*-LAT data are in units of 10^{-7} $\text{ph cm}^{-2} \text{s}^{-1}$. Swift-XRT and UVOT are in units of 10^{-12} and 10^{-11} $\text{erg cm}^{-2} \text{s}^{-1}$ respectively.

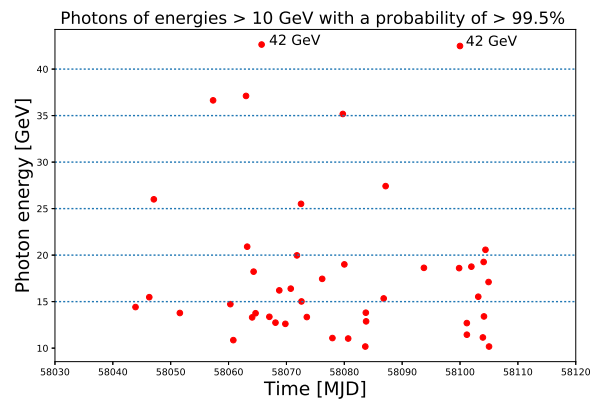


Figure 3. The arrival time of photons of energy > 10 GeV , with probability $> 99.5\%$.

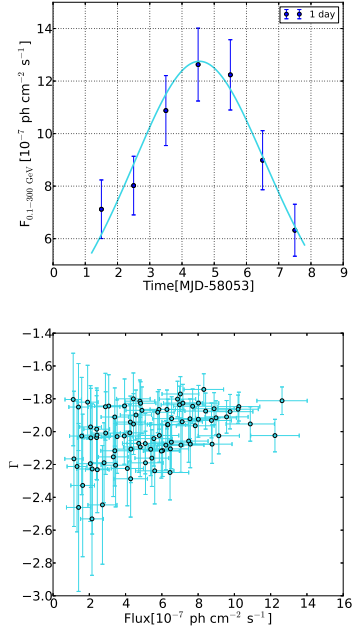


Figure 4. left: Temporal fitting of the flare’s first peak. Right: Photon index is plotted with photon flux to show the brighter and harder trend.

3.3. γ -ray emission region

The γ -ray flare along with photon spectral index is plotted separately in Figure 5. A clear variation in the spectral index is seen during the period (MJD 58040 – MJD 58120). In the pre-flare state (Figure 1), between MJD 57980 to MJD 58040, the source is almost in quiescence with an average flux of $9.35 \times 10^{-8} \text{ ph cm}^{-2} \text{ s}^{-1}$ and the average photon index is 2.38. Once the source is in full fledge flaring episode 58054 to 58110. The average photon flux rises to $6.94 \times 10^{-7} \text{ ph cm}^{-2} \text{ s}^{-1}$ with an average spectral index of 1.96. The maximum flux attained during flaring episode is $12.63 \times 10^{-7} \text{ ph cm}^{-2} \text{ s}^{-1}$ at MJD 58057.5 with photon index 1.81 (Figure 5). The fastest variability time from the 1-day binning light curve (Figure 5) is estimated here, by using the following expression

$$F(t_2) = F(t_1) \cdot 2^{(t_2 - t_1)/t_d}, \quad (2)$$

where $F(t_1)$ and $F(t_2)$ are the fluxes measured at time t_1 and t_2 respectively and t_d represents the doubling/halving timescale of flux. A range of variability time is found, from one day to a few days. One day is used as the fastest variability time to estimate the size of the emission region, by using the relation

$$R \leq ct_{var} \delta (1+z)^{-1} \quad (3)$$

where, $z = 0.72$ and δ is the Doppler factor. The size of the emission region is found to be $1.88 \times 10^{16} \text{ cm}$, for $\delta = 12.5$ (Zhang et al. 2002; Liodakis et al. 2017) which is close to value ($\delta = 15$) estimated by Ghisellini et al. (1998).

Detection of high energy photons ($> 20 \text{ GeV}$) during the flare of Ton 599 puts a constraint on the location of the γ -ray emission region. Liu & Bai (2006) have estimated the optical depth for gamma-rays with energies 10-100 GeV produced within the BLR. They have found that the BLR is opaque for above $20 \text{ GeV}/(1+z)$

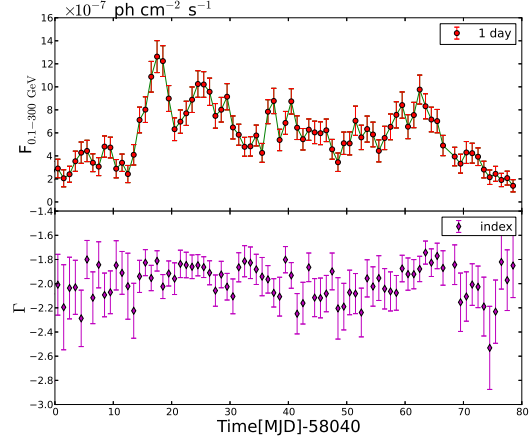


Figure 5. One day bin gamma-ray LC with photon spectral index.

gamma-ray photons. This means that the high energy photons seen during the flare (Figure 3) must have been emitted outside or outer edge of the BLR. Distance (R) of the γ -ray emitting blob from the central super-massive black hole is also estimated by using the relation $R \sim r/\psi$, where ‘ r ’ is the size of the γ -ray emitting region and ψ is the semi-aperture angle of the jet (Foschini et al. 2011). In general, ψ lies between 0.10-0.25 (Ghisellini & Tavecchio 2009; Dermer et al. 2009).

The intrinsic opening angle is estimated from observations by Pushkarev et al. (2009), and they found that the average intrinsic opening angles for a sample of BL Lacs is 2.4 ± 0.6 degree and for quasars is 1.2 ± 0.1 degree. In Pushkarev et al. (2009) sample, Ton 599 is listed as J1156+295, and the intrinsic opening angle is derived as 0.58° . For opening angle 0.58° , the location of emission region is estimated as $3.24 \times 10^{16} \text{ cm}$ which is near the boundary of the BLR (2.4×10^{17} and $2.98 \times 10^{17} \text{ cm}$) dissipation region estimated by Wu et al. (2018) and Pian et al. (2005) respectively. Therefore, at the time of 42 GeV of photon emission during the flare, γ -ray emission region must have been located outside or at the edge of the BLR. Pushkarev et al. (2017) have also calculated the intrinsic opening angle for 65 sources from MOJAVE-1 sample. They have found that the intrinsic opening angles for these 65 sources lie between 0.1° to 9.4° , with a median of 1.3° . The range of opening angle suggest the location of the emission region must lie between 1.88×10^{17} to $2.00 \times 10^{15} \text{ cm}$. The location of the emission region estimated for Ton 599 ($3.24 \times 10^{16} \text{ cm}$) is found to be in this range.

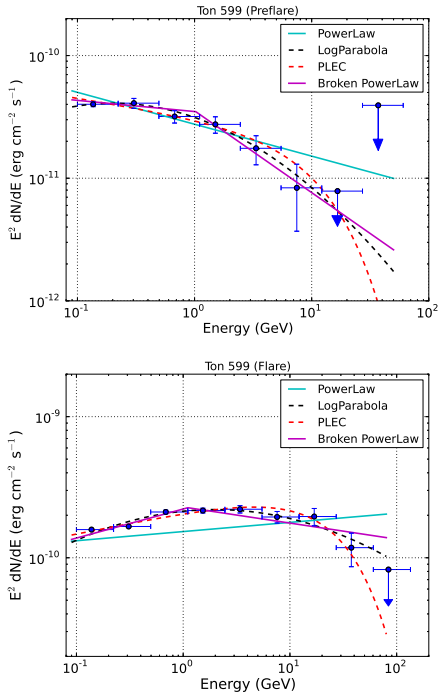
3.4. Spectral Analysis

The spectral analysis of pre-flare and flare observed at the end of 2017 is presented in this section. Likelihood analysis is done with four different spectral models mentioned in Prince et al. (2018). The SEDs data points are fitted with four spectral models (PL, LP, PLEC, and BPL) discussed in Prince et al. (2018), the fitted parameters are presented in Table 2, and the plots are shown in Figure 6. Fitting the gamma-ray SEDs data points with these four models will help us to constrain the gamma-ray emission region. Inside the BLR, photon-photon pair production ($\gamma \gamma \rightarrow e^+e^-$) can attenuate the gamma-ray flux and as a result, we expect to see a break in gamma-

Table 2

Parameters obtained from the spectral analysis fit, for the different models PL, LP, PLEC, and BPL, for the pre-flare and flare by using the Likelihood analysis method. $\Delta\text{Log}(\text{likelihood})$ is estimated with respect to the $\text{Log}(\text{likelihood})$ of the PL fit.

PowerLaw (PL)						
Activity	$F_{0.1-300 \text{ GeV}}$ ($10^{-7} \text{ ph cm}^{-2} \text{ s}^{-1}$)	Γ		$-\text{Log}(\text{likelihood})$	$\Delta\text{Log}(\text{likelihood})$	
Pre-flare	2.45 ± 0.15	2.26 ± 0.05		99810.26		
Flare	11.00 ± 0.02	1.94 ± 0.01		183323.43		
LogParabola (LP)						
	α	β				
Pre-flare	2.27 ± 0.01	2.08 ± 0.09	0.10 ± 0.04	99806.43	-3.83	
Flare	10.40 ± 0.02	1.79 ± 0.02	0.06 ± 0.01	183294.99	-28.44	
PLExpCutoff (PLEC)						
	Γ_{PLEC}	E_{cutoff}				
Pre-flare	2.36 ± 0.02	2.15 ± 0.08	12.51 ± 7.60	99808.07	-2.19	
Flare	10.60 ± 0.02	1.85 ± 0.01	30.00 ± 0.08	183291.44	-31.99	
Broken PowerLaw (BPL)						
	Γ_1	Γ_2	E_{break}			
Pre-flare	2.30 ± 0.02	2.09 ± 0.08	2.67 ± 0.17	1.10 ± 0.17	99806.06	-4.2
Flare	10.50 ± 0.02	1.79 ± 0.03	2.11 ± 0.04	1.11 ± 0.22	183297.07	-26.36

**Figure 6.** SEDs of pre-flare and flaring period of Ton 599

ray spectrum. A break in the gamma-ray spectrum can be examined by fitting the gamma-ray SEDs data points with LP/BPL/PEC. While in other case when the emission region is outside the BLR or within the molecular

torus (MT) a simple PL could be a good fit to the SED data points. In Table 2, the quality of the unbinned fit is presented by the $\text{Log}(\text{likelihood})$ value and the model with a large value of $\Delta\text{Log}(\text{likelihood})$, with respect to PL, preferred over the lower one. Overall all the three models LP, PLEC, and BPL are compatible with the SEDs data points. A clear spectral hardening is seen with increasing flux when the source travels from pre-flare to flaring state. For PL, during pre-flare to flare the flux rises from 2.45 ± 0.15 to 11.00 ± 0.02 ($\times 10^{-7} \text{ ph cm}^{-2} \text{ s}^{-1}$) and the spectral index (Γ) changes from 2.26 ± 0.05 to 1.94 ± 0.01 . A break in the γ -ray spectrum is seen during the flare while fitting the SED with BPL. It shows the rising spectrum before the break and falling spectrum after the break. Before the break, the BPL photon index Γ_1 is 1.79, the break energy E_{break} is 1.11 GeV, and after the break, BPL photon index Γ_2 is 2.11. This suggests that the peak of the IC mechanism probably lie in the LAT energy band and the shape of the γ -ray spectrum likely reflects the distribution of emitting electrons.

3.5. Fractional variability (F_{var})

Variability seen at all frequencies and timescales in blazars is completely a random process. It is more prominent during the flare, and the flare profiles depend on the particle acceleration and energy dissipation. The amplitude of variation depends on the jet parameters like magnetic fields, viewing angle, particle density and the efficiency of acceleration (Kaur & Baliyan 2018). To determine the variability amplitude in all energy band, good quality data is required across the entire electromag-

Table 3
Fractional variability is estimated for time interval 57980 to 58120.

Waveband	F_{var}	$err(F_{var})$
γ -ray	0.730	0.019
U	0.514	0.008
B	0.503	0.007
V	0.485	0.008
W1	0.537	0.009
M2	0.531	0.007
W2	0.536	0.008
OVRO (15 GHz)	0.071	0.004

netic spectrum. Observation of Ton 599 across the entire electromagnetic spectrum makes it possible to determine the variability amplitude using the fractional root mean square (rms) variability parameter (F_{var}) introduced by Edelson & Malkan (1987); Edelson et al. (1990).

Fractional variability is used to compare the variability amplitudes across the entire electromagnetic spectrum and can be estimated by using the relation given in Vaughan et al. (2003),

$$F_{var} = \sqrt{\frac{S^2 - \sigma^2}{r^2}} \quad (4)$$

$$err(F_{var}) = \sqrt{\left(\sqrt{\frac{1}{2N}} \cdot \frac{\sigma^2}{r^2 F_{var}}\right)^2 + \left(\sqrt{\frac{\sigma^2}{N}} \cdot \frac{1}{r}\right)^2} \quad (5)$$

where, $\sigma_{XS}^2 = S^2 - \sigma^2$, is called excess variance, S^2 is the sample variance, σ^2 is the mean square uncertainties of each observations and r is the sample mean.

The fractional variability for all the wavebands is mentioned in Table 3. It is clear that source is most variable in γ -ray and then UV, Optical and radio (at 15 GHz). Because of the large error bar in the X-ray data, I could not estimate the fractional variability. The F_{var} is 0.73 in γ -ray, 0.53 in UVW2-band, 0.50 in optical B-band and 0.07 in radio (at 15 GHz). It is found that F_{var} is increasing with energy, suggesting that a large number of particles are producing the high energy emission. Similar behavior of fractional variability is also seen for other FSRQ like CTA 102 by Kaur & Baliyan (2018), where they found a trend of large fractional variability towards higher energies. Increase in fractional variability is also seen in TeV blazar, Patel et al. (2018) and Sinha et al. (2016) have noted an increase in fractional variability from radio to X-rays and decrease in high energy part from γ -rays to Hard X-rays. An opposite trend was also reported by Bonning et al. (2009), where variability amplitudes decrease towards shorter wavelength (IR, Optical, and UV), which suggests the presence of steady thermal emission from the accretion disk.

3.6. Correlations

From Figure 2, it is very clear that the flares in γ -ray, X-ray, Optical and UV band are mostly correlated. The radio flare at 15 GHz noted after few days of γ -ray flare. The detailed study about correlations has been done in this particular section. A cross-correlation study of flux variations in different energy band can give an idea of whether emissions in different bands are coming from the

same emission region in the jet and if not then it gives an indication of a relative distance between the emitting zones. So, I have done the correlation studies using the discrete correlations function (zDCF) formulated by Edelson & Krolik (1988). It provides insight about the emission in different energy band. Let's suppose there are two discrete data sets a_i and b_j and they have standard deviation σ_a and σ_b , the discrete correlations for all measured pairs (a_i - b_j) is defined as,

$$UDCF_{ij} = \frac{(a_i - \bar{a})(b_j - \bar{b})}{\sqrt{(\sigma_a^2 - e_a^2)(\sigma_b^2 - e_b^2)}} \quad (6)$$

Where each pairs are associated with a pairwise lag $\Delta t_{ij} = t_j - t_i$. The parameters e_a and e_b are the measurement errors associated with data sets a_i and b_j respectively. Binning the UDCF_{ij} in time will directly result in DCF(τ). Averaging the UDCF_{ij} over M number of pairs for which $(\tau - \Delta\tau/2) \leq \Delta t_{ij} < (\tau + \Delta\tau/2)$,

$$DCF(\tau) = \frac{1}{M} UDCF_{ij}, \quad (7)$$

and the error on DCF is defined as,

$$\sigma_{DCF}(\tau) = \frac{1}{M-1} \left\{ \sum [UDCF_{ij} - DCF(\tau)] \right\}^{1/2} \quad (8)$$

Discrete correlations function (DCF) are plotted in Figure 7 for different combinations like γ -X-ray, γ -Swift M2, γ -Swift V and γ -OVRO (15 GHz).

In γ -X-ray correlations it is found that there is no time lag between γ -ray and X-ray emission and the maximum DCF is 0.55. The strong correlation and zero time lag between γ -ray and X-ray suggests that the emissions are originated from the same region or very close-by region. A Significant correlation has been seen in γ -ray and optical (V-band) emission with a small time lag and the peak DCF is noted as 0.85. Similar kind of behavior is also seen in γ -ray and UV (M2 filter) emission with peak DCF 0.90. Larionov et al. (2013) also found small lag in γ -ray and optical emission for S50716+71 and at the same time they also noted an emergence of radio knot K3. Finally, they have concluded that all these events are co-spatial. Similar results were also noticed for CTA 102 (Larionov et al. 2016; Kaur & Baliyan 2018) during the outburst of 2012 and 2017 with remarkable similarity in two energy emission. Significant correlation and small time lag in γ -ray and optical/UV can be explained by leptonic models, where it is assumed that the optical/UV emission is mostly the synchrotron emission from the jets and the γ -ray emission is the product of inverse Compton (IC) scattering of optical/UV photons by the relativistic electrons present in the jets.

It is believed that γ -ray emission is product of IC scattering of soft photons off the same electrons producing the optical radiation, then its variations are expected to be simultaneous or delayed with respect to the optical radiation, and it can be the result of modeling the non-thermal flares with shocks in a jet model (Sikora et al. 2001; Sokolov et al. 2004; Sokolov & Marscher 2005). This kind of behaviour is already seen in few other blazars like 4C 38.42 (Raiteri et al. 2012), 3C 345 (Schinzel et al. 2012) and

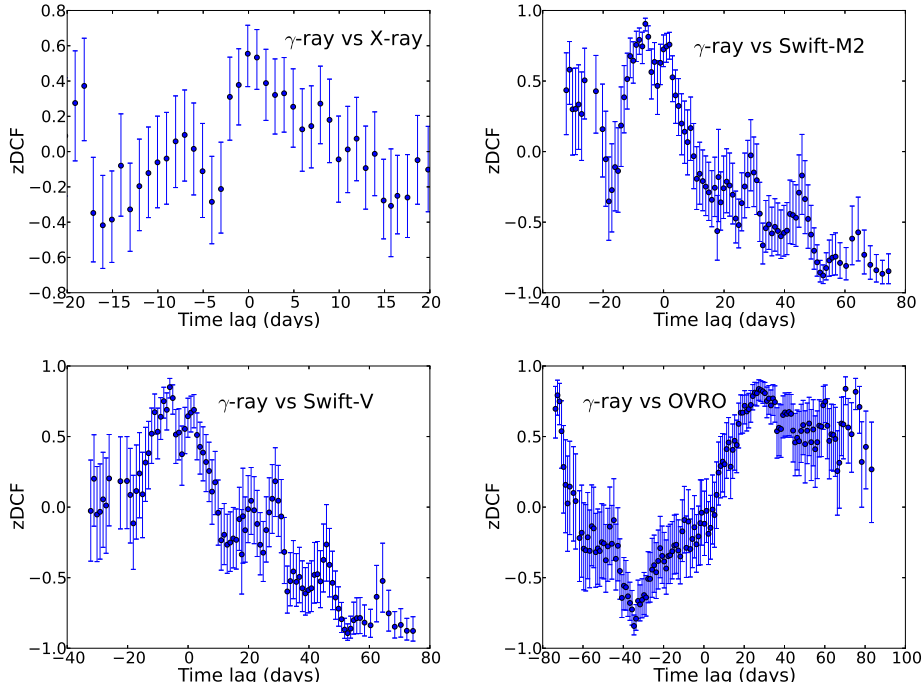


Figure 7. DCF is plotted for all four combinations: γ -X-ray, γ -Swift-M2, γ -Swift-V, γ -OVRO(15 GHz) from left to right, for the flare of Ton 599 during end of 2017.

in 3C 454.3 (Bonning et al. 2009; Vercellone et al. 2010; Raiteri et al. 2011). Interestingly, the opposite behaviour is also seen, where γ -ray is leading with optical radiation, in few blazars e.g. FSRQ PKS 1510-089 (Abdo et al. 2010; D’Ammando et al. 2011) and in 3C 279 (Hayasida et al. 2012). It can be explained by considering fast decay in energy density of external seed photon, responsible for the IC emission, along with the jet axis, compared to the decay in magnetic field energy density which is responsible for the synchrotron emission.

A complex correlation between gamma-ray and optical radiation has also been addressed, by Marscher (2014), by considering the effect of turbulence in the jets. Since the magnetic field is embedded in the jets so turbulence in jets can cause turbulent magnetic field which will affect mostly the synchrotron emission and that can lead to the optical variability while turbulent magnetic field cannot affect the γ -ray radiation. In other words, γ -ray emission region could be better aligned along the line of sight, which can lead to a higher Doppler factor of high energy flux, as compared to optical emitting region.

A correlation study between γ -ray and IR/optical/UV has also been done before for some of the blazar e.g. Bonning et al. (2009); Vercellone et al. (2009); Raiteri et al. (2011); Jorstad et al. (2013); Larionov et al. (2013) and Cohen et al. (2014), where they suggested the co-spatial origin of γ -ray and IR/optical/UV emission. It is also possible that the nature of the correlation between two emitted fluxes changes with epochs and it can be seen as an involvement of different processes and/or different particle population during the high activity.

The right plot of lower panel of Figure 7 shows the correlation between γ -ray and radio (OVRO; 15 GHz). A lag of 27 days in the radio emission at 15 GHz is noted

with DCF peak of 0.84. Since the γ -ray and optical emission is well correlated with a small time lag which suggests that radio emission also lags with optical by the same amount as with γ -ray.

Time delay uncovered by DCF analysis can relate to the relative location of the emission region at different wavebands, which depends on the physics of the jets and high energy radiation mechanisms. The lag of 27 days in the radio emission with γ -ray/optical clearly says that these two emissions are from two different locations in the jets. The observed time lag between γ -ray and radio can be used to determine the distance between two emitting regions by using the equation given in Fuhrmann et al. (2014)

$$\Delta r_{\gamma,r} = \frac{\beta_{app} c \Delta t}{\sin \theta}, \quad (9)$$

Where θ = viewing angle of the source, β_{app} = apparent jet speed, and Δt = observed time lag. Using $\Delta t = 27$ days, and $\theta = 4.3$ degree, $\beta_{app} = 16.13$ from Liodakis et al. (2017), I found $\Delta r_{\gamma,r} \sim 5$ pc. This means the radio emitting region is located far away from the AGN central engine. It is possible that the high energy and radio emission region have different apparent speed as well as different viewing angle which further implies that they have different Doppler factor. A similar situation is also observed by Raiteri et al. (2013) for BL Lacertae, where they found a lag of 120-150 days between γ -ray/optical to radio and the distance between two emitting region in a range of 6.5 to 8.2 pc. Rani et al. (2014) have also found a time lag of 82 days between γ -ray and radio emission for S5 0716+714, the distance between two emission region is estimated in the range 2.9 - 4.4 pc (Rani et al. (2015), for $\beta_{app} = 6 - 8$ c and viewing angle (θ) = 6 - 9 degree).

Alternatively, Flares which are delayed and appear late at lower frequencies can be seen as a clear indication of opacity effects, in the context of shock-in-jet model (Marscher & Gear 1985; Valtaoja et al. 1992), due to synchrotron self-absorption. A shock is formed close to the core where the jet is optically thick to radio frequencies but transparent to high energy, and a component at the core of the jet producing optical/ γ -ray flare, propagates along the jets, and after sometime jet becomes optically thin to detect the radio flare.

4. CONCLUSIONS

During the end of 2017 blazar Ton 599 went into a long flaring episode throughout the entire electromagnetic spectrum. Flaring was first reported in γ -ray followed by the other wavebands. A long delay in the radio flare was observed by OVRO at 15 GHz as seen from Figure 2. Ton 599 was not much variable in X-ray but its variability can be seen in γ -ray and UV/optical. In γ -ray, during the flaring episode a maximum flux 12.63×10^{-7} was noticed with photon index 1.81 and a clear brighter and harder spectral behavior is seen (Figure 4). Large variations in DoP and PA are seen during the flaring period, which can be explained by the shock-in-jet model. Almost all the peaks of the flare show symmetric profile. The rise and decay time of one of the peak is found to be 2.22 ± 0.14 and 2.30 ± 0.13 days. Two 42 GeV of photons are detected during the flaring period with a probability of 99.7% and 99.8%. For the γ -rays the size of the emission region is estimated as 1.88×10^{16} cm by using 1-day as the fastest variability time and the location of the emission region is found to be at the outer edge of the BLR. Gamma-ray SED for pre-flare and flare are fitted with four spectral models PL, LP, PLEC, and BPL. For a flare, PLEC gives a better fit to the SED data points over LP and BPL. A break in the γ -ray spectrum at 1.11 GeV is seen, which suggest the peak of the IC mechanism lies in the LAT energy band and the shape of the photon spectrum likely reflects the distribution of emitting electrons. Ton 599 has shown a trend of high variability with increasing energy. A strong correlation has been seen between γ -X-ray, γ -UV, γ -Optical, and γ -radio (15 GHz). A good correlation with the lag of a few days suggests the γ -ray and optical/UV are co-spatial. On the other hand, a lag of 27 days has been observed between γ -ray and radio (15 GHz) emission, suggesting the presence of two different emission zones. The separation between these two emissions region is estimated as ~ 5 pc. Detailed gamma and radio observations are needed to probe the two different emission region and a multi-wavelength spectral energy distributions (SEDs) analysis is also required for better constraints on the different emission mechanisms that are taking place in the jets of blazar Ton 599.

Acknowledgements : Author thanks the referee for valuable comments to improve the paper and also thanks to Simran Singh for proof reading. This work has made use of public *Fermi* data obtained from FSSC. This research has also made use of XRT data analysis software (XRTDAS) developed by ASI science

data center, Italy. Archival data from the Steward observatory is used in this research. This research has made use of data from the OVRO 40-m monitoring program (Richards et al. 2011) which is supported in part by NASA grants NNX08AW31G, NNX11A043G, and NNX14AQ89G and NSF grants AST-0808050 and AST-1109911.

REFERENCES

- Abdo, A. A., Ackermann, M., et al. 2010, ApJ, 722, 520
 Abdo, A. A., et al. ApJ, 721, 1425
 Atwood, W. B., Abdo, A. A., et al., 2009, ApJ, 697, 1071
 Acero, F., Ackermann, M., et al., 2015, ApJS, 218, 23
 Aharonian, F., Akhperjanian, A. G., et al. 2007, ApJ, 664, L71
 Bonning, E. W., Bailyn, C., et al. 2009, ApJ, 697, L81
 Botcher, M., 2007, Ap&SS, 309, 95
 Breeveld, A. A., Landsman, W., et al., 2011, arxiv, 1358, 373-376
 Casadio, C., Gomez, J. L., et al. 2015, ApJ, 813, 51
 Chiaberge, M. & Ghisellini, G., 1999, MNRAS, 306, 551
 Cohen, D. P., Romani, R. W., et al. 2014, ApJ, 797, 137
 D’Ammando, F., et al. 2011, A&A, 529, A145
 Dermer, C. D., Finke, J. D., et al. 2009, ApJ, 692, 32
 Edelson, R. A., & Krolik, J. H., 1988, ApJ, 333, 646
 Edelson, R. A., & Malkan, M. A., 1987, ApJ, 323, 516
 Edelson, R. A., Krolik, J. H., & Pike, G. F., 1990, ApJ, 359, 86
 Fuhrmann, L., Larsson, S., et al. 2014, MNRAS, 441, 1899
 Foschini, L., Ghisellini, G., et al. 2011, A&A, 530, A77
 Ghisellini, G., Celloti, A., et al. 1998, MNRAS, 301, 451-468
 Ghisellini, G., & Tavecchio, F., 2009, MNRAS, 397, 985
 Hayasida, M., et al. 2012, ApJ, 754, 114
 Jorstad, S. G., Marscher, A. P., et al. 2013, ApJ, 773, 147
 Kalberla, P. M. W., Burton, W. B., et al., 2005, aap, 440, 775-782
 Kaur, N., Baliyan, K. S., 2018, <https://arxiv.org/abs/1805.04692>
 Konigl, A., 1981, ApJ, 243, 700
 Larionov, V. M., Jorstad, S. G., et al. 2013, ApJ, 768, 40
 Larionov, V. M., Villata, M., et al., 2016, MNRAS, 461, 3047-3056
 Liodakis, I., Marchili, N., et al. 2017, MNRAS, 466, 4625-4632
 Liu, H. T., & Bai, J. M., 2006, ApJ, 653, 1089
 Marscher, A. P., et al. 2008, Nature, 452, 966
 Marscher, A. P. & Gear, W. K., 1985, ApJ, 298, 114
 Marscher, A. P., 2014, ApJ, 780, 87
 Patel, S. R., Shukla, A., et al., 2018, A&A, 611, A44
 Pian, E., Falomo, R., & Treves, A., 2005, MNRAS, 361, 919-926
 Prince, R., Raman, G., et al. 2018, ApJ, 866, 16
 Pushkarev, A. B., Kovalev, Y. Y., Lister, M. L., & Savolainen, A., 2009, A&A, 507, L33-L36
 Pushkarev, A. B., Kovalev, Y. Y., & Lister, M. L., 2010, ApJ, 722, L7
 Pushkarev, A. B., Kovalev, Y. Y., Lister, M. L., & Savolainen, A., 2017, MNRAS, 468, 4992
 Raiteri, C. M., Villata, M., et al. 2011, A&A, 534, A87
 Raiteri, C. M., 2012, A&A, 545, A48
 Raiteri, C. M., Villata, M., 2013, MNRAS, 436, 1530
 Ramkrishnan, V., Leon-Tavares, J., et al. 2014, MNRAS, 445, 1636
 Rani, B., Krichbaum, T. P., et al. 2014, A&A, 571, L2
 Rani, B., Krichbaum, T. P., et al. 2015, A&A, 578, A123
 Richards, J. L., Max-Moerbeck, W., et al. 2011, ApJS, 194, 29
 Roming, P. W. A., Kennedy, T. E., et al., 2005, ssr, 120, 95-142
 Schlafly, E. F., Finkbeiner, D. P., 2011, ApJ, 737, 103
 Schinzel, F. K., Lobanov, A. P., et al. 2012, A&A, 537, A70
 Sikora, M., Blazejowski, M., Begelman, M. C., 2001, ApJ, 554, 1
 Sinha, A., Shukla, A., Saha, L., et al., 2016, A&A, 591, A83
 Smith, P. S., Montiel, E., et al. 2009, ArXiv: 0912.3621
 Sokolov, A., Marscher, A. P., McHardy, I. M., 2004, ApJ, 613, 725
 Sokolov, A., & Marscher, A. P., 2005 ApJ, 629, 52
 Urry, C. M., & Padovani, P., 1995, PASP, 107, 803
 Valtaoja, E., Terasranta, H., Urpo, S., et al. 1992, A&A, 254, 71
 Vaughan, S., Edelson, R., et al. 2003, MNRAS, 345, 1271
 Vercellone, S., Chen, A. W., et al. 2009, ApJ, 690, 1018
 Vercellone, S., 2010, ApJ, 712, 405
 Wu, L., Wu, Q., et al. 2018, ApJ, 852, 45
 Zhang, L. Z. & Fan, J. H., et al. 2002, PASJ, 54, 159-169